

Diffuse optical fluorescence imaging: sensitivity to heterogeneities and autofluorescence

Frédéric Leblond, Nicolas Robitaille, Simon Fortier, Niculae Mincu, Jean Brunette, Mario Khayat

ART Advanced Research Technologies Inc., 2300 Alfred-Nobel Blvd., Saint-Laurent, CANADA H4S 2A4

fleblond@art.ca

Introduction

Diffuse optical fluorescence imaging is based on the use of fluorescent probes that can be excited by light in the near-infrared (NIR) and visible parts of the electromagnetic spectrum. Imaging with NIR and visible light presents several advantages related to their non-invasive character and low operational cost compared to more standard imaging methods.

When designing a small-animal imaging system having tomographic capabilities, it is critical to evaluate as well as maximize the sensitivity for detecting specific distributions of fluorescent molecules. Sensitivity is significantly affected by the internal structure and geometry of the biological sample of interest. Another intrinsic factor impacting the sensitivity of a system is the ubiquitous degradation of the signal-to-background ratio (SBR) caused by the autofluorescence of tissues. Our analysis shows how the complex anatomical structure of a small animal and the autofluorescence phenomenon influence data acquired with diffuse optical fluorescence systems.

Small-animal Heterogeneities

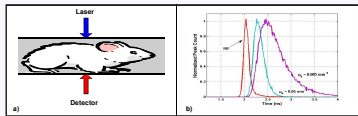


Figure 1: We consider data acquired with systems based on two different illumination-collection technologies: continuous wave (CW) and time-resolved (TR). (a) Schematic depiction of the source-detector geometry (transmission mode) used to perform a scan. (b) simulated temporal point-spread functions (TPSF) for diffusive samples with different optical properties ($\mu_a = 1 \text{ mm}^{-1}$). The impulse response function (IRF) of the system is represented by the red curve. CW signals (not shown) correspond to straight lines extending over the full 12.5 ns time-window.

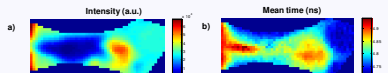


Figure 2: Images produced using TR mouse data (light emission and collection at 690 nm) for co-axial acquisition performed in transmission mode: a) intensity (normalized first moment of the TPSF), b) mean time of photon arrival (normalized first moment of the TPSF). As depicted in Figure 1a), the animal was placed in a tank filled with optical matching liquid having optical properties $\mu_a = 0.03 \text{ mm}^{-1}$ (absorption coefficient) and $\mu_s = 1 \text{ mm}^{-1}$ (reduced scattering coefficient).

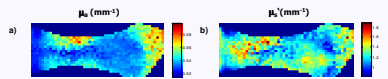


Figure 3: Effective optical properties (μ_a and μ_s) of tissues are important input parameters for algorithms designed to process optical fluorescence data. Given light transport can be approximately modeled by solutions to the diffusion equation, the optical properties can be determined by curve fitting of the TPSFs. The images show the effective optical contrast present in a mouse: a) absorption coefficient, b) reduced scattering coefficient. Absorption varies from 0.015 mm^{-1} to 0.097 mm^{-1} while scattering ranges from 0.81 mm^{-1} to 1.88 mm^{-1} .

Numerical Simulations

Simulation results consist of optical data generated with the NIRFAST software package [1,2]. This software uses a finite-elements method (FEM) to find numerical solutions to the diffusion equation as well as for more complicated cases involving fluorescent sources. Although limited to the diffusive light transport regime, NIRFAST is general in that it allows the generation of solutions associated with heterogeneous media having optical contrast in absorption and reduced scattering, as well as in fluorophore lifetime and concentration.

Detection Geometries

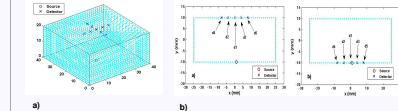


Figure 4: Light emission and detection configurations considered for the simulations. a) Example of a detection geometry used to perform 3D simulated tomography scans with signal acquisition in transmission mode. The detectors are arranged in a cross-shape geometry with 4 mm spacing between closest neighbors. b) Detection geometries considered for 2D simulations: transmission configuration (left) and reflection mode configuration (right). Tomography data is generated by scanning a detection configuration over the region-of-interest.

Depth Sensitivity

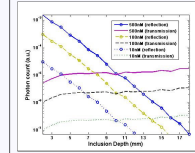


Figure 5: Relative sensitivity (measured as CW signal on a logarithmic scale) to fluorescent molecules as a function of center-of-mass depth, for various molar concentrations. The molecules are distributed within a sphere with a radius of 1.5 mm. Curves showing a flatter response to depth variations are related to the transmission configuration while the exponentially decreasing behavior characterizes the reflection mode collection geometry.

Autofluorescence and Contrast-detail

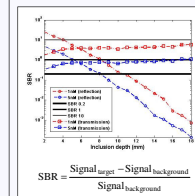


Figure 6: Autofluorescence consists of photons emanating from unlabeled tissues and/or ingested food. As shown on the figure, it can limit the detection capabilities of a diffuse optical imager. Oils, pigments and proteins endogenous to mice all contribute to whole body autofluorescence. The figure shows SBR as a function of depth (molecules distributed within a sphere with a 1.5 mm-radius having 100 nM concentration) for both transmission and reflection detection channels. Autofluorescence is modeled as a homogeneous fluorescent background with different concentration levels (curves for 1 nM and 5 nM are shown).

$$SBR = \frac{\text{Signal}_{\text{target}} - \text{Signal}_{\text{background}}}{\text{Signal}_{\text{background}}}$$

Heterogeneities and Tomography Data

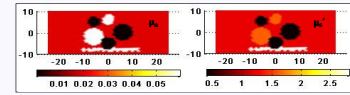


Figure 7: Schematic depiction of a diffusive medium (corresponding to level 4 below) considered for 2D simulations performed to evaluate the impact of optical property heterogeneities on a full tomography data set. The sample is a slab with 20 mm thickness and background optical properties $\mu_a = 0.02 \text{ mm}^{-1}$ and $\mu_s = 1 \text{ mm}^{-1}$ (left image: absorption coefficient map, right image: reduced scattering coefficient map).

Heterogeneities	$\mu_{a,max} (\text{mm}^{-1})$	$\mu_{s,max} (\text{mm}^{-1})$	$\Delta\mu_a$	$\mu_{a,max} (\text{mm}^{-1})$	$\mu_{s,max} (\text{mm}^{-1})$	$\Delta\mu_s$
Level 1	0.015	0.03	0.015	1.0	1.5	0.5
Level 2	0.01	0.04	0.03	0.8	2.0	1.2
Level 3	0.005	0.05	0.045	0.6	2.4	1.8
Level 4	0.0005	0.06	0.055	0.4	2.8	2.4

Table 1: Minimum, maximum and range values for the absorption and reduced scattering coefficients associated with the four heterogeneous media considered in the 2D simulations (see Figure 7).

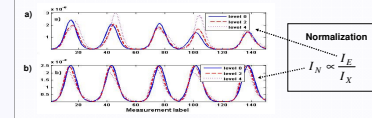


Figure 8: CW tomography data set generated by scanning the transmission detection configuration depicted in Figure 4b) over the heterogeneous samples represented in Figure 7. Fluorescent molecules are distributed within a 1.5 mm-radius sphere with 100 nM concentration. The center-of-mass is located 5 mm under the surface: a) raw fluorescence data (I_{ij}), b) Born-normalized data (I_{ij}^B). I_{ij} represents data acquired at the fluorophore excitation wavelength. Curves are shown for three levels of optical property heterogeneities, i.e., levels 0 (homogeneous medium), 2 and 4. Each peak represents a different detector (d1 to d5 from left to right).

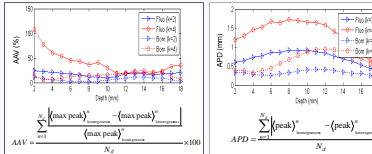


Figure 9: Figures of merit illustrating the impact of Born normalization [3] on tomography data for light collection using the transmission configuration shown on Figure 4b): a) average amplitude variation (in %) b) average peak displacement (in mm) as a function of inclusion depth. On each graph, raw fluorescence and Born-normalized fluorescence curves are shown for heterogeneous levels of 2 and 4. N_d is the total number of detectors.

Experimental Evaluation

A heterogeneous phantom was designed as shown in Figure 10 (see Table 2 for specifications). Four cylindrical Cy5.5 inclusions were embedded in an autofluorescing polyurethane matrix in order to simulate fluorescent regions inside a diffusive medium. CW illumination of the sample was performed at 650 nm with 1 mm resolution along both x and y axes with a detection configuration as shown in Figure 1a). The maximum laser power available during the scans was 38 mW. Two data sets were acquired using different filter configurations: (1) fluorescence data (collection at a wavelength close to the peak of the emission spectrum of the fluorophore), (2) excitation data (collection close to the peak of the excitation spectrum). The resulting images are shown in Figure 11.

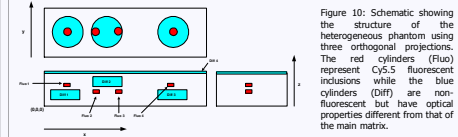


Figure 10: Schematic showing the structure of the heterogeneous phantom using three orthogonal projections. The red cylinders (Fluo) represent Cy5.5 fluorescent inclusions while the blue cylinders (Diff) are non-fluorescent but have optical properties different from that of the main matrix.

Matrix	Excitation (nm)			Emission (nm)			Optical properties (mm ⁻¹)		
	λ	Δ	α	λ	Δ	α	μ_a	μ_s	IT
Fluo	650	10	10	650	30	20	0.02	1.0	...
Diff 1	13	15	7	18	6	0.005	0.5
Diff 2	39	15	15	18	6	0.04	2.0
Diff 3	79	15	7	18	6	0.01	0.5
Diff 4	14	15	13	100	30	1.5
Fluo 1	650	10	10	2
Fluo 2	32	15	9	2
Fluo 3	78	15	11	2
Fluo 4	78	15	11	2

Table 2: Heterogeneous phantom technical specifications. The spatial locations are referenced with respect to the origin (0,0,0) shown in Figure 10.

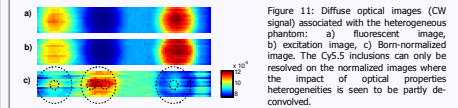


Figure 11: Diffuse optical images (CW signal) associated with the heterogeneous phantom: a) fluorescent image, b) excitation image, c) Born-normalized image. The Cy5.5 inclusions can only be resolved on the normalized images where the impact of optical properties heterogeneities is seen to be partly deconvolved.

Conclusions

Based on numerical simulations, we have shown how non-specific fluorescence can degrade the SBR in fluorescence images. In particular, we found that the sensitivity of imaging devices acquiring data in reflection is superior to an acquisition performed in transmission when the fluorescent molecules are close to the surface. However, we find that transmission systems are better suited for tomography applications since their sensitivity does not vary significantly with depth.

An approximation that is often made when designing algorithms for processing diffuse optical data is that the biological samples of interest have homogeneous optical properties. Based on synthetic and experimental data, we have shown how this assumption can degrade the correspondence between an actual tomography data set and one computed using a homogeneous model. We provided evidence that data normalization can significantly improve on this situation.

References

[1] S. C. Davis, H. Dehghani, J. Wang, S. Jiang, B. W. Pogue, K. D. Paulsen, "Image-guided diffuse optical fluorescence tomography implemented with Laplacian-type regularization," *Opt. Express* 15, 4066-4083 (2007).
 [2] S. C. Davis, B. W. Pogue, H. Dehghani, K. D. Paulsen, "Contrast-detail analysis characterizing diffuse optical fluorescence tomography image reconstruction," *J. Biomed. Opt.* 10, 050501-1-3 (2005).
 [3] V. Ntziachristos and R. Wehrli, "Experimental three-dimensional fluorescence reconstruction of diffuse media by use of a normalized Born approximation," *Opt. Lett.* 12, 893-895 (2001).